INT. J. NUM. METH. HEAT FLUID FLOW, VOL. 4, 413–424 (1994)

SELECTED PAPER FROM THE BAIL VI CONF., COLORADO, U.S.A., 1992.
SPECIAL EDITOR PROF. J. J. H. MILLER

SIMULATION OF VORTICAL STRUCTURES IN A JET DIFFUSION FLAME

V. R. KATTA, L. P. GOSS

Systems Research Laboratories, Inc., A Division of Arvin/Calspan, 2800 Indian Ripple Road, Dayton, OH 45440-3696, USA

AND

W. M. ROQUEMORE

Wright Laboratory, Aero Propulsion and Power Directorate, Wright-Patterson Air Force Base, OH 45433-7103, USA

ABSTRACT

The dynamics of a transitional propane jet diffusion flame with a fuel-jet velocity of 2.2 m/s has been studied using an implicit, third-order-accurate, upwind numerical scheme. The large-scale vortices outside the flame surface and the small-scale ones inside were simulated simultaneously, and their interactions with the flame surface were investigated. Numerical experiments were conducted to gain insight into the influence of buoyancy and shear-layer forcing on the development of the outer and inner vortices. In the presence of buoyancy forces, the outer vortices developed as part of the solution, and the vortex-crossing frequency was approximately 15 Hz. The inner structures were manifested from a weak perturbation in the vorticity that was introduced at the nozzle exit, and, at 185 Hz, these vortices were found to travel farther downstream. It was also found that the inner vortices do not play a role in the formation of the outer vortices, and vice versa. However, the growth of the inner vortices in the downstream locations is strongly influenced by the slowly moving outer vortices.

KEY WORDS Jets Diffusion flame Vortices Upwind

INTRODUCTION

The existence of vortex structures inside and outside the flame surface that become a characteristic of transitional jet diffusion flames was first observed by Yule *et al.*[1] and subsequently by Eickhoff[2] and Roquemore *et al.*[3]. The inner small-scale structures in flames that develop due to the instability of the jet shear layer are different from those in cold jets[4]. The vortices in a reacting flow grow very slowly and maintain their identities over a long distance, as compared to the rapid formation and growth of these structures in cold flows. However, in both reacting and cold flows, the frequency of the inner vortices depends on the velocity gradient across the shear layer and the viscosity. The large vortices in flames, on the other hand, are generated outside the flame surface and are analogous to the structures observed along heated vertical walls[5]. These slowly moving outer vortices are, in general, not sensitive to the fuel-jet velocity, fuel composition, or geometrical dimensions. Buckmaster and Peters[6] have provided a theoretical background for this phenomenon by isolating the natural convective flow from the forced one.

0961–5539/94/040413–12$2.00

Received February 1993
Revised September 1993

Both the outer and inner vortices interact with the flame surface and create wrinkles on it. With the help of high-speed movies, Chen *et al.*[7] confirmed that low-frequency flame oscillation (flame-flicker) is the result of the convective motions of the wrinkled flame and the large outer vortices. These visualizations also indicated that the shape and rotational characteristics of the inner vortices seem to change at certain locations inside the flame, which suggests that the development and growth of the inner vortices are influenced by the motion of the outer vortices.

Numerical studies by Davis *et al.*[8] and Ellzey *et al.*[9] have demonstrated that the large vortices outside the flame result from the buoyant acceleration of the hot gases along the flame surface. In the present paper, direct numerical simulations are presented which capture the temporal and spatial development of both the outer and the inner vortex structures of a transitional propane jet diffusion flame. Computational experiments were performed to investigate the importance of buoyancy and shear-layer forcing on the development of the outer and inner vortices. Changes in the growth of the inner vortices due to the presence of the outer vortices are also discussed.

MATHEMATICAL MODEL

The diffusion flame studied in this work is formed between a central propane jet and a very low speed co-annular air flow. The time-dependent governing equations, expressed in cylindrical coordinates (z, r), are:

$$\frac{\partial \rho}{\partial t} + \frac{\partial \rho u}{\partial z} + \frac{1}{r}\frac{\partial (r\rho v}{\partial r} = 0 \tag{1}$$

$$\frac{\partial(\rho\Phi)}{\partial t} + \frac{\partial(\rho u\Phi)}{\partial z} + \frac{\partial \rho v\Phi}{\partial r} = \frac{\partial}{\partial z}\left(\Gamma^{\Phi}\frac{\partial \Phi}{\partial z}\right) + \frac{\partial}{\partial r}\left(\Gamma^{\Phi}\frac{\partial \Phi}{\partial r}\right) - \frac{\rho v\Phi}{r} + \frac{\Gamma^{\Phi}}{r}\frac{\partial \Phi}{\partial r} + S^{\Phi} \tag{2}$$

where ρ represents density; u and v are the axial and radial components of the velocity vector, respectively; and p is the pressure. The general form of (2) represents the axial momentum, radial momentum, species, or energy-conservation equation, depending on the variable used in place of Φ. The conserved scalar variables β_1 and β_2 defined as

$$\beta_1 = \frac{\alpha Y_O + Y_F^i - Y_F}{\alpha Y_O^i + Y_F^i}, \quad \text{and} \quad \beta_2 = \frac{h - h_O^i + (Y_F/\alpha)Q}{(Y_F^i/\alpha)Q + h_F^i - h_O^i},$$

are used to represent the species mixture fraction and enthalpy, respectively. Here α is the fuel-oxidizer ratio $(v_F M_F / v_O M_O)$; Y_m and h_m are the mass fraction and enthalpy of the mth species, respectively; h is the mixture enthalpy; Q is the heat release per unit mass of oxygen consumed; M is the molecular weight; and the superscript i represents the fuel-jet and air-flow values. The chemical reaction between the fuel and the oxygen is assumed to occur at an infinitely fast rate, yielding an infinitely thin sheet of flame at:

$$\beta_1 \equiv \beta_1^* = \frac{Y_F^i}{\alpha Y_O^i + Y_F^i}.$$

The transport coefficients Γ^{Φ} and the source terms S^{Φ} that appear in (2) are given in *Table 1*. The body force term due to the gravitational field is included in the axial-momentum equation. Here μ is the viscosity of the mixture; D is the local binary diffusion coefficient between any two species; ρ_0 is the density of air; and g is the gravitational acceleration. The system of governing equations is completed using the state equation:

$$p = \rho T R_0 \left\{\frac{Y_F}{M_F} + \frac{Y_O}{M_O} + \frac{Y_P}{M_P} + \frac{Y_I}{M_I}\right\} \tag{3}$$

Table 1 Transport coefficients and source terms appearing in governing equations

Φ	Γ^{Φ}	S^{Φ}
u	μ	$-\frac{\partial p}{\partial z}+(\rho_0-\rho)g+\frac{\partial}{\partial z}\left(\mu\frac{\partial u}{\partial z}\right)+\frac{\partial}{\partial r}\left(\mu\frac{\partial v}{\partial z}\right)+\frac{\mu}{r}\frac{\partial v}{\partial z}-\frac{2}{3}\left\{\frac{\partial}{\partial z}\left(\mu\frac{\partial u}{\partial z}\right)+\frac{\partial}{\partial z}\left(\mu\frac{\partial v}{\partial r}\right)+\frac{\partial}{\partial z}\left(\mu\frac{v}{r}\right)\right\}$
v	μ	$-\frac{\partial p}{\partial r}+\frac{\partial}{\partial z}\left(\mu\frac{\partial u}{\partial r}\right)+\frac{\partial}{\partial r}\left(\mu\frac{\partial v}{\partial r}\right)+\frac{\mu}{r}\frac{\partial v}{\partial r}-2\mu\frac{v}{r^2}-\frac{2}{3}\left\{\frac{\partial}{\partial r}\left(\mu\frac{\partial u}{\partial z}\right)+\frac{\partial}{\partial r}\left(\mu\frac{\partial v}{\partial r}\right)+\frac{\partial}{\partial r}\left(\mu\frac{v}{r}\right)\right\}$
β_1	ρD	0
β_2	ρD	0

where R_0 is the universal gas constant; and T is the temperature. The subscript I in the above equation represents nitrogen which is assumed to be an inert gas in the present simulation.

Temperature- and species-dependent thermodynamic and transport properties are used in this formulation. The enthalpy of each species is calculated from polynomial curve-fits, while the viscosity of the individual species is estimated from the Chapman–Enskog collision theory[10]. The binary diffusion coefficient between any two species on the fuel side of the flame is assumed to be identically equal to that of the fuel and nitrogen. Similarly, on the oxidizer side of the flame, it is assumed identical to that of the oxidizer and nitrogen. The Chapman–Enskog theory and the Lennard–Jones potentials have been used to estimate the above two binary diffusion coefficients.

Numerical scheme

An orthogonal, staggered grid system with rapidly expanding cell sizes in both the z and r directions is utilized. The governing equations are integrated using an implicit QUICKEST (Quadratic Upstream Interpolation for Convective Kinematics with Estimated Streaming Terms) numerical scheme[11,12] which is third-order accurate in both space and time and has a very low numerical diffusion error. After rearrangement of terms, the finite-difference form of (2) for the variable Φ at a gird point P can be written as an algebraic equation as follows:

$$A_P\Phi_P^{N+1}+A_{z^{++}}\Phi_{z^{++}}^{N+1}+A_{z^{+}}\Phi_{z^{+}}^{N+1}+A_{z^{-}}\Phi_{z^{-}}^{N+1}+A_{z^{--}}\Phi_{z^{--}}^{N+1}+A_{r^{++}}\Phi_{r^{++}}^{N+1}$$
$$+A_{r^{+}}\Phi_{r^{+}}^{N+1}+A_{r^{-}}\Phi_{r^{-}}^{N+1}+A_{r^{--}}\Phi_{r^{--}}^{N+1}=S_P^{\Phi}+\Delta t\cdot\rho_P\Phi_P^{N} \quad (4)$$

The time increment, Δt, is determined from the stability constraint and maintained as a constant during the entire calculation. The superscripts N and $N+1$ represent the known variables at the Nth time step and the unknown variables at the $(N+1)$th time step, respectively; the subscripts z^+ and z^- indicate the values at the grid points immediately adjacent to point P in the positive and negative z-directions, respectively. Similarly, the subscripts z^{++} and z^{--} represent the values at two grid points away from P in the respective directions. The coefficients A and the terms on the right hand side of (4) are calculated from the known flow variables at the Nth time step. Although, the above equation is written in general form, care must be exercised while generating the finite-difference schemes for the u and v momentum equations because of the staggered grid adopted. The four equations represented by (4) are solved individually using an iterative ADI (Alternative Direction Implicit) technique. This involves obtaining solutions for pentadiagonal matrices in the z and r directions iteratively, until the total residual drops below a specified value. Although the momentum and scalar equations represented by (4) are solved independently, a consistent sequence should be followed for simulating time-dependent reacting flows. In the present simulation the equations for β_1 and β_2 are solved first, and then the temperature and density at the $(N+1)$th time step are obtained. Based on the previous

density, the u and v momentum equations are solved next. The pressure field at every time step is accurately calculated by simultaneously solving the system of algebraic pressure Poisson equations at all grid points using the LU (Lower–Upper) decomposition technique.

Initial and boundary conditions

The flowfield considered in the present study has vortical structures of two different scales. While the smaller-scale vortices develop inside the flame surface along the shear layer of the fuel jet, the larger-scale outer vortices form outside the flame surface. The computational domain and the boundary conditions employed to capture these vortical structures are shown in *Figure 1*. The outer boundaries II and IV (cf. *Figure 1*) of the computational domain are located sufficiently far from the nozzle exit (40 nozzle diameters) and symmetry axis (15 nozzle diameters), respectively to minimize the propagation of disturbances into the region of interest. Flat velocity profiles are used at the fuel and air inflow boundaries. The outflow boundary in these flows is the most difficult one to treat because the flow leaving this boundary continuously evolves in time as the large outside and small inside vortices cross this boundary. A simple extrapolation procedure with weighted zero- and first-order terms was used to estimate the flow variables on the boundary in the present calculations. The weighting functions, w_1 and w_2 (cf. *Figure 1*), are selected by the trial-and-error approach, and the main criterion used is that the vortices crossing the outflow boundary should leave smoothly without being distorted.

RESULTS AND DISCUSSION

The inflow conditions used in the present calculations are for a laboratory flame studied experimentally by Roquemore *et al.*[3]. A vertically mounted jet diffusion flame was established by burning pure propane emerging from a 10-mm-diameter contoured nozzle. Flat initial velocity profiles with measured average velocities of 2.22 m/s and 0.15 m/s were used in the calculations at the exit of the fuel nozzle and the annular duct, respectively.

Development of vortices

Laboratory experiments on this flame indicate that vortices having two different scales (referred to as large- and small-scale) can develop when the fuel jet velocity is greater than 1 m/s. According to Buckmaster and Peters[6], the large-scale vortices that are located outside the flame surface are small perturbations amplified by a modified Kelvin–Helmholtz-type instability. In their analysis they separated the natural convection of the hot gases due to buoyancy from the forced convective flow and obtained this modified instability. The small-scale vortices are usually enclosed within the flame; hence, they are often referred to as inner vortices. It is speculated that these inner vortices are generated by the flow perturbations at the nozzle exit and amplified by the Kelvin–Helmholtz-type flow instability of the fuel-jet shear layer. The issues concerning the inner and outer vortices are difficult to address experimentally because of the inherent noise in the flow systems. On the other hand, numerical experiments can offer dissectomy of the complex flowfield resulting from different external forces.

Simulations of Davis *et al.*[8] and Ellzey *et al.*[9] indicate that the outer vortices on the flame form when the gravity force is included in the calculations. Similarly, Katta *et al.*[11] showed that the inner vortices do not become established without introducing noise into the fuel-jet shear layer. Therefore, four different calculations (identified as *Flames 1–4*) were performed in the present study to gain insight into the factors that might influence the development and growth of the vortices in the flame under study. The gravity term in the axial-momentum equation was neglected in the first two cases, and shear-layer perturbations were not introduced in the first and third calculations. Results in the form of iso-temperature contours are plotted in *Figures*

2(a)–2(d). When both gravity and shear-layer perturbations were absent in the *Flame-1* calculation, the solution converged to a steady flame, as seen in *Figure 2(a)*. The possibility that the inner structures generate the outer structures may be ruled out as a result of the second calculation (*Flame 2*). Velocity perturbations of ~0.3% in magnitude and at a frequency of 185 Hz were introduced at the shear layer near the nozzle exit in this calculation. Inviscid stability analysis[13] suggests that the most amplified frequency for the co-annular jet shear layer considered is ~400 Hz. In actual calculations, the perturbations introduced at this frequency did not travel beyond a few nozzle diameters downstream. This could be due to the viscosity of the combustion products. However, the most amplified frequency in these viscous calculations is determined by repeating several calculations and varying the perturbation frequency. At 185 Hz the disturbances travelled farther downstream and developed into a train of inner vortices. The highly viscous fluid resulting from the combustion along the flame surface is entering into the inner vortices and causing them to dissipate at $z = 100$ mm. When the buoyancy force was neglected in this simulation, even the inner vortices did not cause the outer vortices to form (*Figure 2(b)*). However, the flame surface in the downstream locations exhibits weak oscillations, with scales on the order of those of the outer vortices. These oscillations may be due to another type of flow instability which is developing in the low-density flame zone.

When the buoyancy term was activated in the axial-momentum equation, the flame began to oscillate immediately and quickly settled into periodic oscillations, as seen in *Figure 2(c)*. It is important to note that no artificial perturbation was used in this calculation (*Flame 3*). In the presence of a gravity force, the acceleration of hot gases along the flame surface generated the outer structures as part of the solution. The frequency corresponding to the passage of the outer vortices is ~15 Hz. Although the entire flow including the fuel-jet shear layer is oscillating at this low-frequency, it did not initiate the small-scale inner structure; therefore, the potential core remained laminar. In the last calculation (*Flame 4*), the shear-layer perturbations introduced at

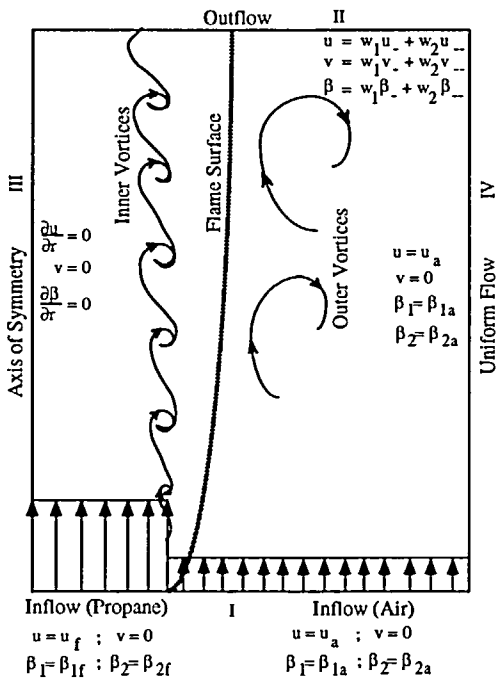

Figure 1 Computational domain and boundary conditions used in calculations

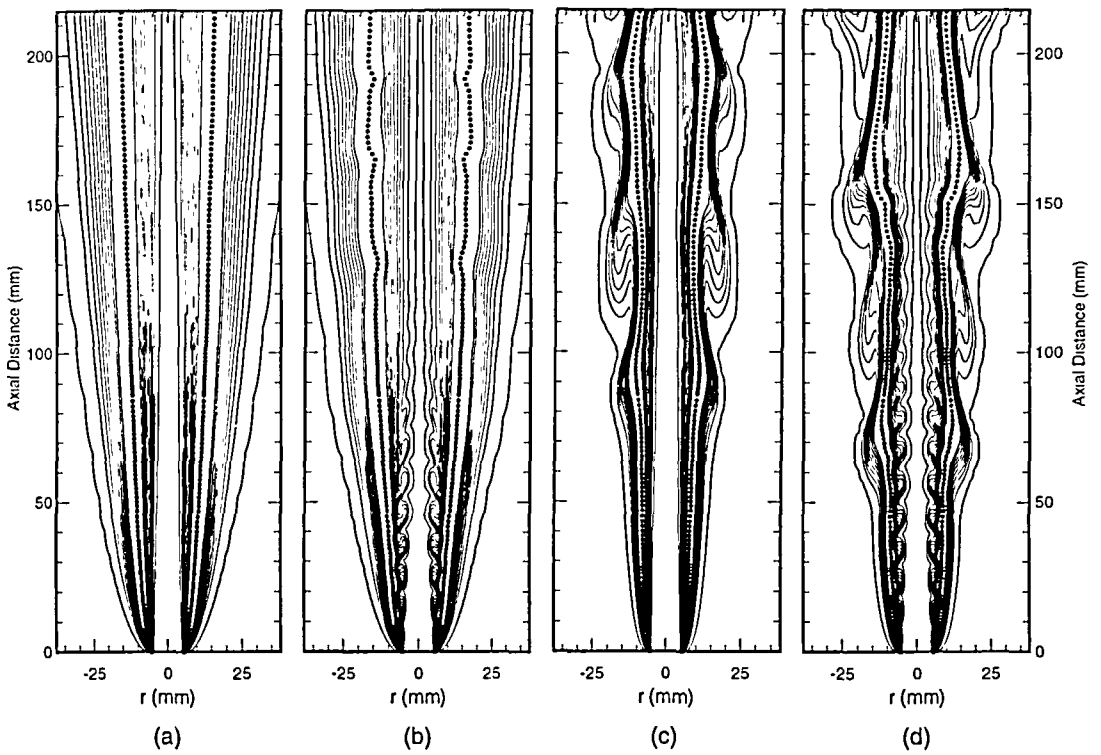

Figure 2 Iso-temperature contours of propane jet diffusion flame obtained from different calculations. Solid circles indicate stochiometric flame surface. Flame in absence of buoyancy forces (a) without and (b) with shear-layer perturbations. Flame under influence of buoyancy (c) without and (d) with shear-layer perturbations

185 Hz developed into long coherent inner structures. This flame appears to be very similar to the laboratory flame[3] and captures its salient features such as the existence of outer and inner structures, longer coherence length for the inner vortices, and relaminarization (losing flow instabilities) of the potential core downstream of $z = 160$ mm. The outer vortices in this flame seem to form earlier than those in the flame without the inner vortices (*Flame 3*).

Influence of double-vortex structure on flame

The radial distributions of temperature and axial velocity at an axial location of 100 mm are compared for different cases in *Figures 3* and *4*, respectively. Since *Flame 1* is a steady flame without inner or outer vortices, the RMS (Root Mean Square) values for this case are zero. The flame surface in this case (*Figure 3(a)*) is located farther away from the center than that in the experiment, and both the temperature and velocity are poorly predicted; these results indicate the importance of buoyancy in this transitional jet flame. The predictions of the current model (*Flame 4*) are in good agreement with the experimental data. The inflection points in the temperature profiles (at $r = 13$ mm in *Figures 3(a)* and *3(b)*) that arise from the motion of the outer vortices are correctly predicted. However, inside the flame the temperature measurements show higher average and RMS values. It is not clear what additional transport mechanism is leading to the enhanced combustion inside the flame. One speculation is that the fine-scale turbulence originating from the nozzle walls is increasing the mixing between the fuel and the oxidizer. However, some degree of uncertainty is associated with temperature measurements (based on the temperature of the nitrogen molecules) inside the flame because of the scarcity of

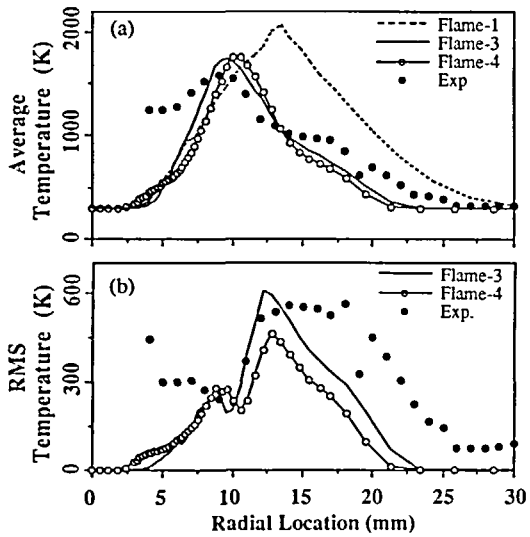

Figure 3 Radial distributions of computed and measured temperature at $z = 100$ mm. (a) Average; (b) RMS

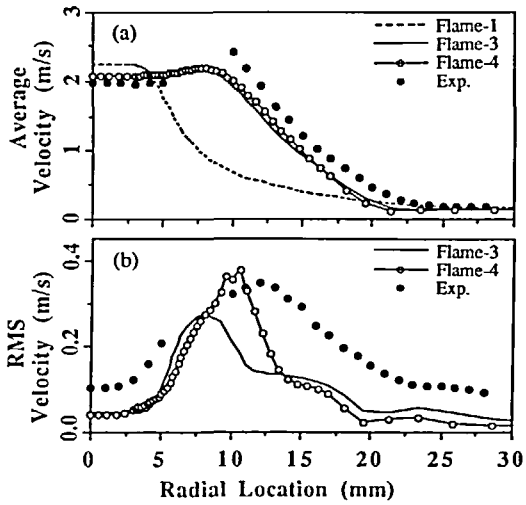

Figure 4 Radial distributions of computed and measured axial velocity at $z = 100$ mm. (a) Average; (b) RMS

the nitrogen molecules there. Closer agreement for the predicted velocities can be seen in *Figures 4(a)* and *4(b)*. The potential core emanating from the 5-mm-radius nozzle is decaying quickly in the nonbuoyant flame calculation (*Flame 1*). The acceleration of hot gases due to buoyancy in *Flames 3* and *4* reduced the velocity gradient to almost zero at the edge of the potential core. This led to a much slower growth rate for the inner vortices in the case of *Flame 4*, as compared to that of the nonbuoyant case, *Flame 2* (cf. *Figure 2*). Although the presence of the inner vortices in *Flame 4* improved the predictions of the average temperature and velocity, their impact on the overall flame seems to be very small up to $z = 100$ mm. This is to be expected since in diffusion flames, the high-temperature surface separates the fuel and the oxidizer. The internal

structures formed along the edge of the potential core which is well inside the flame surface do not enhance mixing between the fuel and the oxidizer; instead, they improve mixing of burnt products with the fuel. This results in only small changes in the temperature and velocity distributions inside the flame.

Temperature evolutions and the corresponding pdf's (probability density functions) at two axial locations ($z = 50$ and 150 mm) for the *Flame-4* case are plotted in *Figures 5* and *6*, respectively. At the former axial location, the inner vortices are stronger and the outer vortices weaker than the respective ones at the latter axial location. The computed temperature data along the radial direction at these axial locations are first recorded over several flame-flicker cycles. The time evolution of the temperature is then obtained by plotting constant-temperature contours. Data for about one flickering cycle (~80 ms) are shown in *Figures 5(a)* and *6(a)*. The pdf plots (*Figures 5(b)* and *6(b)*) are obtained by calculating the probability density of the temperature at each radial location from the recorded data and then drawing constant-probability contour lines. The convergence of contour lines at $r = 16$ mm in *Figure 6(b)* indicates that the vortex at this axial location is well separated from the flame. The bi-modal probability distribution of temperature at a given radial location is due to the flame oscillation or flicker which, in turn, results from the convective motion of the vortices. The radial movements of the flame surface (width of the pdf plots in *Figure 5(b)* and *6(b)* at peak temperature) at $z = 50$ and 150 mm are about 1.2 and 2.8 mm, respectively.

Rotation of the fluid in the outer vortex is such that it pulls the hot gases from the flame surface on the leading side of the vortex and brings the outside air into the flame zone on the trailing side. On the other hand, the inner vortices add fuel to the flame zone on the leading side and take away combustion products on the trailing side. In both situations, wrinkles (cf. *Figures 2(d)*, *5(a)*, and *6(a)*) having scales corresponding to the interacting vortices form on the

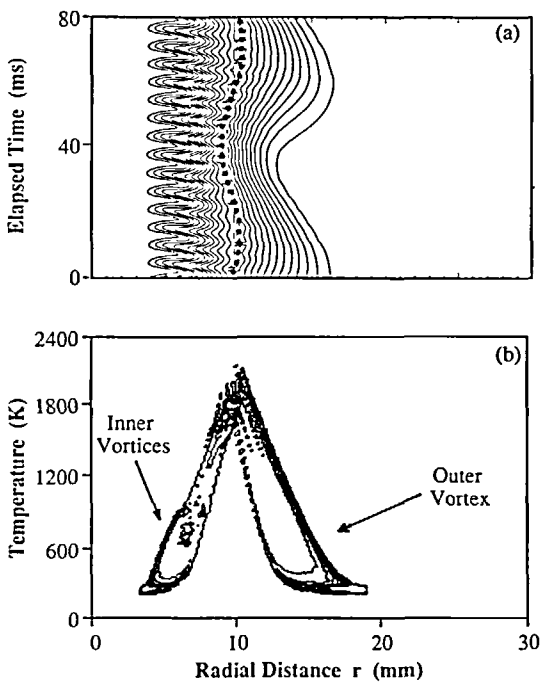

Figure 5 (a) Temperature history of computed flame at $z = 50$ mm. (b) Iso-probability-density contours obtained from temperature data

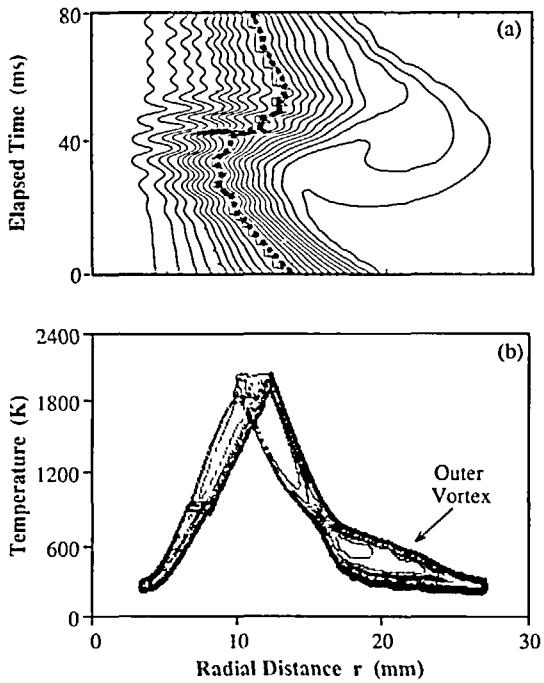

Figure 6 (a) Temperature history of computed flame at $z = 150$ mm. (b) Iso-probability-density contours obtained from temperature data

flame surface. The small-scale wrinkles on the flame surface in the calculations occur at the instant when the flame is pushed closer to the potential core by the outer vortex. Although these small-scale wrinkles are weak and not a major contributor to the RMS profiles in *Figure 3(b)*, they have been recently observed by Chen *et al.*[14] in the studies of this flame using the thin-filament-pyrometry technique. However, at higher jet flow velocities, the inner vortices grow much more rapidly and may interact with the flame surface strongly.

Evolution of vortices

Frequency spectra at different axial locations for the flame under consideration were obtained from the temperature data collected at a radial location within the shear layer ($r = 5$ mm) and are shown in *Figure 7*. Two different modes of shear-layer oscillations are evident from these spectra. The lower-frequency component results from the convective motion of the outer vortices and the higher-frequency one from the inner vortices. At $z = 50$ and 100 mm, the outer vortices create weaker fluctuations within the shear layer than the inner ones. This process is reversed at $z = 200$ mm, indicating relaminarization of the shear layer. Absence of frequencies other than the natural 15 Hz and the forced 185 Hz suggests that no vortex merging is taking place in this flame. However, the peaks—especially at 185 Hz—become broad at the downstream locations. This could be due to the influence of the outer vortices on the inner ones. The squeezing action of the outer vortex not only increases the local axial velocity but also brings the viscous fluid of the flame zone closer to the inner vortices, which could affect the growth of the nearby inner vortex. Therefore, the instantaneous inner-vortex structure shown in *Figure 2(d)* might change when the outer vortices are located at a different position at another instant of time.

The evolution of the inner and outer vortices is visualized in *Figure 8* using a particle-tracking technique. During the calculations for *Flame 4*, massless particles were released in the shear

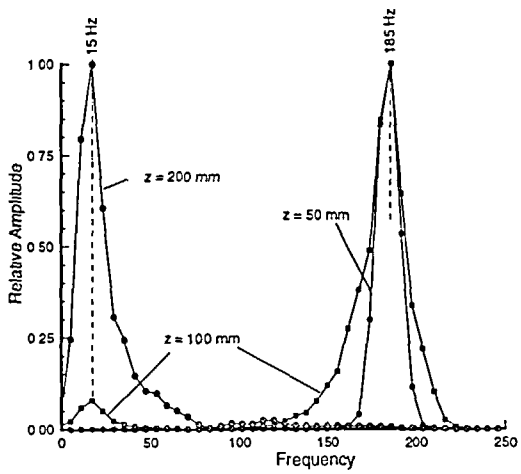

Figure 7 Frequency spectra at different axial locations obtained from temperature data

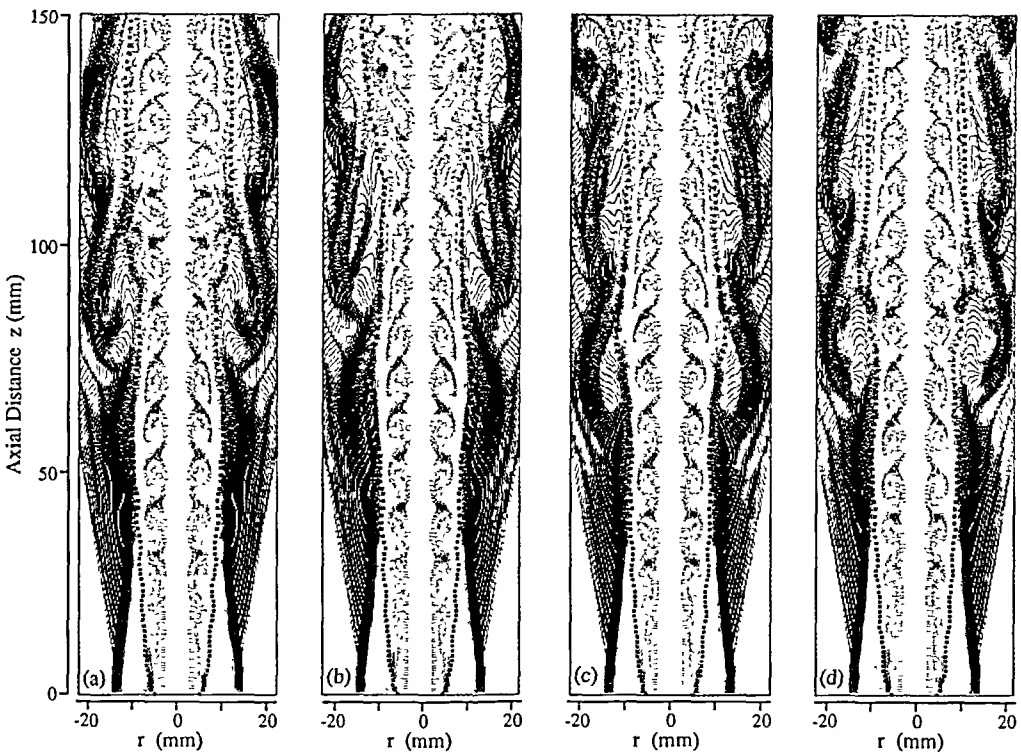

Figure 8 Evolution of inner and outer vortices visualized by particle traces. Massless particles are continuously released at the nozzle exit and along inclined line in annular air flow. Instantaneous locations of all particles released from the same location are plotted with same color. Black solid squares indicate stoichiometric flame surface. (a) $t = 0$; (b) $t = 17.7$ ms; (c) $t = 35.5$ ms; (d) $t = 53.2$ ms

layer at the nozzle exit and along the inclined line in the outer-annulus air flow. At a given instant of time, the locations of all particles released from a common point were plotted with the same color. Therefore, the particles represented with the color green in *Figures 8(a)–8(d)* were released inside the flame and at the nozzle exit. Similarly, the particles represented with the color blue were released at a location farther outside the flame and in the annular air flow. Four instantaneous images with a phase difference of 17.75 ms, which is about one-fourth of the flame-flicker cycle, are shown in *Figures 8(a)–8(d)*. The vortex structures are more easily identified in these plots than in the contour plot of *Figure 2(d)*. The solid squares indicate the instantaneous location of the stoichiometric flame surface. The particles that were released in the annular-air flow cross the flame surface, which shows an important characteristic of a diffusion flame—that the external fluid is continuously entrained into the flame zone[15].

The shape of the inner vortices up to $z = 50$ mm is very similar in all four phases. In these figures no effort was made to match the phases of the inner vortices. At this location, the outer vortex begins to affect the flame. It is clear that the inner vortices are stretched axially, while the flame is squeezed by the outer vortex (at $z = 80$ mm in *Figure 8(a)*, at $z = 110$ mm in *Figure 8(b)*, and at $z = 150$ mm in *Figure 8(c)*). Similarly, when the flame bulges out, the inner vortices are pulled radially or, in other words, compressed axially. These structural changes are reflected in the broadening of the frequency spectra in *Figure 7*. The inner vortices of this flame exhibit an interesting characteristic. At $z = 145$ mm and $t = 17.75$ ms, the inner vortices change their direction of rotation[16]. This phenomenon occurs due to a combination of the two fluid accelerations which result from (1) the rotational motion of the buoyancy-generated outside vortex and (2) the buoyancy force on the hot gases. The change in rotation of the inner vortices was also observed in the experiments[3] at about the same height from the nozzle exit.

CONCLUSION

A third-order accurate, upwind numerical scheme is used to capture the complex dynamics of a transitional jet diffusion flame. The two distinct vortex structures—one inside and the other outside the flame surface—were simulated simultaneously, and the flame surface was found to be located between these vortex structures. Buoyancy is responsible not only for generating the outside structures but also for maintaining the coherence (or identity) of the inner structures over a long distance downstream. The low-frequency perturbations (~ 15 Hz) generated by the motion of the outer vortices do not initiate the development of the inner vortices. When the fuel-jet shear layer was forced with higher-frequency perturbations, the response was observed to be maximum at 185 Hz. Although the inner vortices create small wrinkles on the flame surface, their overall impact on the flame is insignificant. The presence of the outer vortices, however, has a significant effect on the development of the inner vortices. When the flame is pulled out by the outer vortex, the nearby inner vortices become compressed axially. In a near-turbulent flame, such compression of vortices results in merging vortices.

ACKNOWLEDGEMENT

This work was supported, in part, by US Air Force Contract F33615-90-C-2033. The authors would like to thank Mrs. M. Whitaker for help in the preparation of the manuscript.

REFERENCES

1 Yule, A. J., Chigier, N. A., Ralph, S., Boulderstone, R. and Ventura, J. Combustion-transition interaction in a jet flame, *AIAA J.*, 19 (6), 752–760 (1981)

2 Eickhoff, H. Instability and coherent structures in jet flames, *Recent Contributions to Fluid Mechanics*, Springer-Verlag, Berlin and Heidelberg, 50–57 (1982)
3 Roquemore, W. M., Chen, L-D., Goss, L. P. and Lynn, W. F. The structure of jet diffusion flames, *Turbulent Reactive Flows, Lecture Notes in Engineering*, **40** (R. Borghi and S. N. B. Murthy, Eds), Springer-Verlag, Berlin, 49–63 (1989)
4 Savas, O. and Gollahalli, S. R. Flow structure in near-nozzle region of gas jet flames, *AIAA J*, **2** (7), 1137–1140 (1986)
5 Holman, J. P., Gartrell, H. E. and Soehngen, E. E. An interferometric method of studying boundary layer oscillations, *J. Heat Trans.*, **82**, 263–264 (1960)
6 Buckmaster, J. and Peters, N. The infinite candle and its stability—A paradigm for flickering diffusion flames, *Twenty-First Int. Symp. on Combustion*, The Combustion Institute, Pittsburgh, PA, 1829–1836 (1986)
7 Chen, L-D., Seaba, J. P., Roquemore, W. M. and Goss, L. P. Buoyant diffusion flames, *Twenty-Second Int. Symp. on Combustion*, The Combustion Institute, Pittsburgh, PA, 677–684 (1988)
8 Davis, R. W., Moore, E. F., Roquemore, W. M., Chen, L-D., Vilimpoc, V. and Goss, L. P. Preliminary results of a numerical-experimental study of the dynamic structure of a buoyant jet diffusion flame, *Combust. Flame*, **83**, 263–270 (1991)
9 Ellzey, J. L., Laskey, K. J. and Oran, E. S. Effects of heat release and gravity on an unsteady diffusion flame, *Twenty-Third Int. Symposium on Combustion*, The Combustion Institute, Pittsburgh, PA, 1635–1640 (1990)
10 Reid, R. C., Prausnitz, J. M. and Poling, B. E. *The Properties of Gases and Liquids*, McGraw-Hill Book Company, New York (1987)
11 Katta, V. R., Goss, L. P. and Roquemore, W. M. Numerical investigations on the dynamic behaviour of a H_2–N_2 diffusion flame under the influence of gravitational force, *AIAA Paper 92-0335*, Reno, NV (1992)
12 Leonard, B. P. A stable and accurate convective modelling procedure based on quadratic upstream interpolation, *Comp. Meth. Appl. Mech. Eng.*, **19**, 59–98 (1979)
13 Michalke, A. and Jermann, G. On the inviscid instability of a circular jet with external flow, *J. Fluid Mech.*, **114**, 343–350 (1982)
14 Chen, L-D. Private communication (University of Iowa, Iowa City, Iowa) (1991)
15 Takahashi, F., Mizomoto, M. and Ikai, S. Structure of the stabilizing region of a laminar jet diffusion flame, *J. Heat Trans*, **110** (2), 192–189 (1988)
16 Katta, V. R. and Roquemore, W. M. Role of inner and outer structures in a transitional diffusion flame, *Comb. Flame*, **92**, 274–282 (1993)